NANO · MICRO small
www.small-journal.com

Enhancing the Microstructure of Perovskite-Inspired Cu-Ag-Bi-I Absorber for Efficient Indoor Photovoltaics

*G. Krishnamurthy Grandhi, Basheer Al-Anesi, Hannu Pasanen, Harri Ali-Löytty, Kimmo Lahtonen, Sari Granroth, Nino Christian, Anastasia Matuhina, Maning Liu, Alex Berdin, Vincenzo Pecunia, and Paola Vivo**

Lead-free perovskite-inspired materials (PIMs) are gaining attention in optoelectronics due to their low toxicity and inherent air stability. Their wide bandgaps (≈2 eV) make them ideal for indoor light harvesting. However, the investigation of PIMs for indoor photovoltaics (IPVs) is still in its infancy. Herein, the IPV potential of a quaternary PIM, Cu_2AgBiI_6 (CABI), is demonstrated upon controlling the film crystallization dynamics via additive engineering. The addition of 1.5 vol% hydroiodic acid (HI) leads to films with improved surface coverage and large crystalline domains. The morphologically-enhanced CABI+HI absorber leads to photovoltaic cells with a power conversion efficiency of 1.3% under 1 sun illumination—the highest efficiency ever reported for CABI cells and of 4.7% under indoor white light-emitting diode lighting—that is, within the same range of commercial IPVs. This work highlights the great potential of CABI for IPVs and paves the way for future performance improvements through effective passivation strategies.

1. Introduction

Artificial indoor lighting, such as white light-emitting diodes (WLED) and fluorescent lamps, is a readily available energy source for the numerous and pervasive smart electronics of our modern environments. While hydrogenated amorphous silicon (a-Si:H) is currently the industry standard light-harvesting material for indoor photovoltaics (IPVs), emerging photovoltaic technologies have recently attracted considerable attention for IPVs due to their higher efficiencies and potentially lower environmental footprint.[1–6] In particular, lead halide perovskite (LHP)-based IPVs have already demonstrated a cutting-edge indoor power conversion efficiency (iPCE) of 40.1%.[5] Yet, the presence of lead in LHPs raises toxicity concerns, even more relevant than for outdoor light-harvesting applications of LHPs. This, therefore, opens an avenue for the design and development of IPVs relying on lead-free perovskites and low-toxicity perovskite-inspired materials (PIM).[6–8] Stable PIM compositions for solar cell applications are mainly based on bismuth (Bi) and antimony (Sb), which are less toxic than lead.[8–12] Importantly, many such PIMs have bandgaps ≈2.0 eV, which enables them to efficiently absorb artificial indoor light, resulting in maximum theoretical iPCEs in the range of 50–60%.[1,8,13] To date, only two PIMs, namely $Cs_3Sb_2Cl_xI_{9-x}$ (bandgap = 1.95 eV) and $AgBiI_4$ (bandgap = 1.8 eV), have been explored for IPVs, leading to iPCEs (≈5%) already in the same range of commercial a-Si-H devices.[8,14] Given these

G. K. Grandhi, B. Al-Anesi, H. Pasanen, N. Christian, A. Matuhina, M. Liu, P. Vivo
Hybrid Solar Cells
Faculty of Engineering and Natural Sciences
Tampere University
P.O. Box 541, Tampere FI-33014, Finland
E-mail: paola.vivo@tuni.fi

H. Ali-Löytty
Surface Science Group
Photonics Laboratory
Tampere University
P.O. Box 692, Tampere FI-33014, Finland

The ORCID identification number(s) for the author(s) of this article can be found under https://doi.org/10.1002/smll.202203768.

DOI: 10.1002/smll.202203768

K. Lahtonen
Faculty of Engineering and Natural Sciences
Tampere University
P.O. Box 692, Tampere FI-33014, Finland

S. Granroth
Department of Physics and Astronomy
University of Turku
Turku FI-20014, Finland

A. Berdin
Smart Photonic Materials
Faculty of Engineering and Natural Sciences
Tampere University
P.O. Box 541, Tampere FI-33014, Finland

V. Pecunia
School of Sustainable Energy Engineering
Simon Fraser University
5118 – 10285 University Drive, Surrey, British Columbia V3T 0N1, Canada

promising, starting results and the considerable potential for improvement toward their ultimate iPCE limits, PIMs provide an attractive avenue for next-generation IPVs. However, novel PIM compositions and advanced control of their crystallization and film morphology optimization are greatly needed to significantly boost the PCE of the corresponding PIM-PVs.

Recently, Sansom et al. have reported a quaternary PIM based on Cu, Ag, Bi, and I with Cu_2AgBiI_6 (CABI) composition.[15] The optoelectronic properties of CABI, such as the direct bandgap and high absorption coefficient (1.0×10^5 cm^{-1}), highlight its potential as a light-harvester for solar cell applications.[15,16] Furthermore, the layered structure of CABI ensures more efficient charge transport than other 0D PIMs.[15,17] Nevertheless, a very modest PCE of 0.43% under AM 1.5G was demonstrated for CABI-based solar cells in the first article on the material.[15] Very recently, the PCE value of 1% was achieved through the surface passivation of CABI layer.[18] Nevertheless, the low solar PV performance can be partly attributed to CABI's bandgap of 2.06 eV, which leads to large optical losses under solar illumination. Moreover, despite the film formation optimization via a proposed two-step annealing,[15,18] the reported CABI films presented numerous pinholes and surface cracks or small size grains of a few hundred nanometers, which may induce shunt leakage effects and are detrimental to charge transport. Therefore, the film growth of CABI must be optimized to achieve smoother films with continuous morphology and large-sized grains.

To advance the optoelectronic performance of CABI, herein we introduce an acid additive, hydroiodic acid (HI), to improve CABI film morphology and the performance of CABI-based photovoltaic cells. CABI being a very recent material, no such additive engineering has been reported to date. We show that an optimal concentration of HI (1.5 vol%) in CABI precursor solution leads to a significant increase in the domain size and surface coverage of CABI in the films. As a result, the optical and photophysical properties of CABI were also improved. When the HI-containing CABI films were tested as absorbers in IPVs for the first time, we achieved a champion PCE approaching 5%. By studying the dependency of the photovoltaic parameters on the light intensity, we identified the current device performance bottlenecks, allowing us to suggest future efforts in effective passivation strategies to further enhance the optoelectronic properties and photovoltaic performance of CABI.

2. Results and Discussion

2.1. Influence of HI Additive on Structural, Morphological, and Optical Properties of CABI

CABI thin films processed with and without the HI additive (the former case being referred to as CABI+HI in the following), were deposited on glass and FTO-coated glass substrates inside a N_2-filled glove box by spin-coating, followed by a two-step thermal annealing in air,[15] first at 50 °C for 50 min and then at 200 °C for 4 min. The optimal concentration of HI in CABI precursor was 1.5 vol% (see details on the optimization and Figures S1 and S2, Supporting Information). The X-ray diffraction (XRD) patterns of the as-fabricated films collected at room temperature (**Figure 1**a) matched those of CABI reported earlier.[15] CABI and CABI+HI crystallize in a highly complex network in the *R*3-*m* space group. Alternating layers of the network comprise octahedral (partially occupied by Ag^+ or Bi^{3+} ions) and tetrahedral sites (partly filled with Cu^+ ions) formed by the cubic close-packed iodide sublattice (Figure 1b). Complete details on CABI crystal structure are found in the work by Sansom et al.[15] We determined the elemental composition of the films by scanning electron microscopy-energy dispersive X-ray spectroscopy (SEM-EDS). SEM-EDS mapping (Figure 1c) shows a uniform distribution of Cu, Ag, Bi, and I. Both CABI and CABI+HI films contain a little excess of Cu, with an overall average composition of $Cu_{2.4}Ag_{1.0}Bi_{0.7}I_{4.8}$ and $Cu_{2.6}Ag_{1.0}Bi_{0.8}I_5$ for CABI and CABI+HI, respectively (see **Table 1**). The presence of excess Cu and lower Bi content in the films is consistent with the previously reported compositions ($Cu_{2.5}Ag_{1.0}Bi_{0.8}I_6$)[15] of CABI and is ascribed to the presence of Cu_2BiI_5 impurities, which can be identified also from the XRD patterns of Figure 1a. The co-existence of the Cu_2BiI_5 impurity phase with the CABI phase was observed also earlier.[15,16] The lower iodine amount detected by SEM-EDS in the bulk of the films can be attributed both to the presence of Cu_2BiI_5 impurity and to the possible depletion of iodine under electron beam exposure during the EDS measurement.[19] Still, the detected iodine concentration is slightly higher for the CABI+HI film. Compared to the bulk composition, the surface compositions (topmost 5–9 nm) of CABI and CABI+HI were strongly depleted in Cu and Ag and enriched in Bi, as determined by X-ray photoelectron spectroscopy (XPS) (see Table 1, and Figures S3–S5 and the detailed surface analysis in the Supporting Information). The surface enrichment of Bi in the samples is considered a surface segregation effect that is driven by the minimization of surface energy.[20] Indeed, the surface energies of metals increase in the order of Bi (0.49 J m^{-2}) < Ag (1.25 J m^{-2}) < Cu (1.79 J m^{-2}).[21] The iodine amount detected by X-ray photoelectron spectroscopy (XPS) was also lower than the expected value. Slightly excess iodine was present on CABI+HI film's surface compared to that of the pristine CABI film. Metal oxide (M-O) formation is also observed at the surfaces, similarly as reported by Hamdeh et al. for BiI_3 film, which was suggested to facilitate the hole extraction improving its photovoltaic device performance.[22]

The SEM study of CABI and CABI+HI reveals that both samples show incomplete surface coverage with many gaps between the CABI domains. When the films were annealed at a temperature of 75 °C, that is, lower than the above-mentioned 200 °C, an increase in smoothness and surface coverage was achieved (Figure S6, Supporting Information), in agreement with the known annealing temperature effect on the film morphology of LHPs.[23] However, at low-temperature annealing, the films suffer from low crystallinity and the presence of many pinholes (Figure S6, Supporting Information). The difference in the surface morphologies of CABI and CABI+HI films at two different annealing temperatures observed by SEM images (Figure 1d and Figure S6, Supporting Information) is further supported by their atomic force microscopy (AFM) topography images, as shown in Figure S7, Supporting Information. The addition of HI promotes the growth of larger crystalline domains for CABI+HI (average size 8.4 μm) compared to CABI

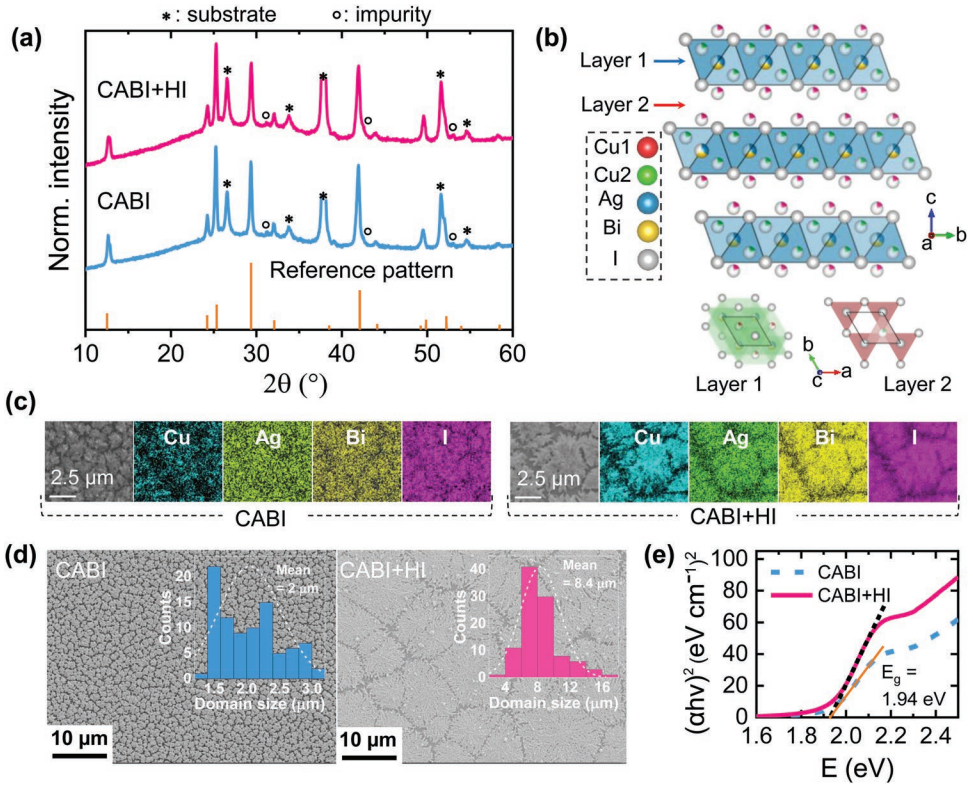

Figure 1. a) XRD patterns of CABI and CABI+HI films deposited on FTO along with the reference pattern of CABI. The highest intense peaks at 25.5°, 29.5° and 42.2° correspond to (012), (104) and (110) crystal planes, respectively. The peaks marked with the asterisk and open circle symbols denote the XRD reflections corresponding to the FTO substrate and impurities, respectively. The substrate's peak at 37.8° is not shown completely. b) Crystal structure of CABI. c) EDS maps of CABI and CABI+HI films showing the distribution of the elements. d) SEM images of CABI and CABI+HI films. Insets are the size distribution of CABI domains in the films. e) Tauc plots of CABI and CABI+HI films.

(2 μm) films (Figure 1d) and, in turn, increases the net surface coverage from 81% (CABI) to 92% (CABI+HI). The thicknesses of CABI and CABI+HI films are nearly equal (values between 275 and 285 nm). This could be due to a solubility enhancement of the precursor upon HI incorporation and control of CABI crystallization dynamics, as found earlier for other PIMs and LHPs.[10,24,25]

CABI+HI film absorbs more strongly than its CABI counterpart (Figure 1e) for photon energies in the range between 2.1 (600 nm) and 2.5 eV (500 nm). Nevertheless, the addition of HI does not influence either the shape of the absorption spectrum or the bandgap of the films (1.94 eV, see Figure 1e). The emission properties of CABI films were earlier discussed by Buizza et al., who found that, when excited at 400 nm, the samples emit as a result of exciton self-trapping (STE) processes.[16] Following this report, we also excited CABI and CABI+HI film at 405 nm, that is, with an energy much above the bandgap, and observed a similar weak and broad emission that peaks at 725 nm (1.7 eV), as shown in **Figure 2**a. Surprisingly, the photoluminescence excitation (PLE) spectrum corresponding to the emission maximum (725 nm) comprises a strong signal at ≈420 nm without any bandgap-related features (Figure S8a, Supporting Information), indicating that the broad emission at ≈725 nm does not arise from the bandgap excitation. The 420 nm feature is also present in the absorption spectrum (Figure S8b, Supporting Information) and a similar feature at 2.9–3.0 eV (≈420 nm) can be found in the CABI film's absorption spectrum reported earlier, too.[15] To confirm the origin of the emission, we collected photoluminescence (PL) spectra of the films upon excitation at different wavelengths of the absorption spectrum and saw that the emission is visible only if the excitation energy is higher than the onset energy of the 420 nm

Table 1. Bulk and surface atomic ratios of CABI and CABI+HI films (M = Cu, Ag, Bi) from EDS and XPS analysis.

	Cu	Ag	Bi	I	O (M–O)
CABI bulk (EDS)	2.4	1	0.7	4.8	–
CABI+HI bulk (EDS)	2.6	1	0.8	5	–
CABI surface (XPS)	0.2	1	3.1	4.5	1.4
CABI+HI surface (XPS)	0.3	1	3.2	5.2	1.4

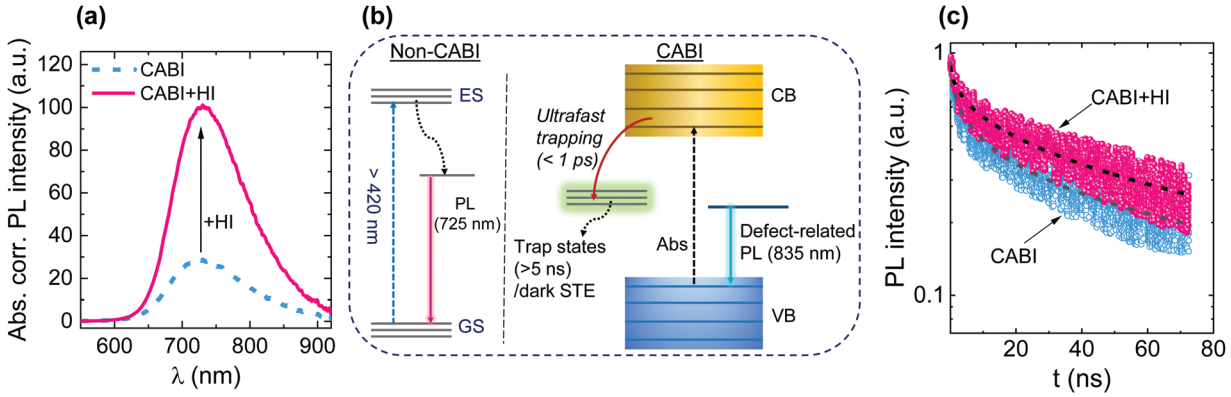

Figure 2. a) PL spectra of CABI and CABI+HI films. b) Scheme of the optical processes observed in the investigated films. c) TRPL decays of CABI and CABI+HI films with the corresponding stretched exponential fits.

feature in the PLE spectrum (Figure S8c, Supporting Information). The PL peak at 725 nm could be assigned to an impurity phase coexisting with CABI or to a defect-related emission, as further discussed in the Supporting Information. The transient absorption (TA) spectroscopy (Figure S9, Supporting Information) characterization of CABI films suggests ultrafast trapping (<1 ps) of charge carriers but provides no evidence for the bright STE state formation in CABI (see the discussion in Supporting Information). The radiative and non-radiative recombination processes in CABI and CABI+HI films observed by the PL and TA study are summarized in Figure 2b.

The presence of the 420 nm absorption feature (origin of the emission) in the external quantum efficiency (EQE) spectra of the solar cells employing CABI or CABI+HI (see **Figure 3**d) hints at the participation of this feature and the corresponding emission to the charge transfer process. To elucidate the effect of HI additive on the photophysical properties of CABI, we compared the steady-state PL spectra and the excited state dynamics of CABI thin films with and without HI (Figure 2a). The PL intensity was four folds higher for the HI-containing CABI film and the analysis of time-resolved PL (TRPL) spectra in Figure 2c shows that the HI addition also prolongs the average charge carrier lifetime of the films (94 and 109 ns for CABI and CABI+HI, respectively). Overall, our study suggests improved radiative recombination upon HI addition.

2.2. The PV Performance of CABI and CABI+HI Devices

To assess the impact of HI addition on device performance, we fabricated n-i-p photovoltaic cells with CABI active layers, with and without HI, and evaluated their respective performance under 1 sun illumination (AM 1.5G, 100 mW cm^{-2}) and low-intensity WLED light (4000 K, 0.46 mW cm^{-2}). The cross-sectional image of a typical device structure, comprising a ≈275-nm-thick CABI layer, compact TiO_2, and doped Spiro-OMETAD (standard electron- and hole-transport layer, ETL and HTL, of high-performance LHP-based solar cells), respectively, is shown in Figure 3a. Details on device fabrication and characterization are provided in the Supporting Information.

Figure 3b shows the statistical distribution of the photovoltaic parameters of CABI and CABI+HI devices under 1 sun illumination. The champion devices delivered a PCE of 0.60% and 1.30% for CABI and CABI+HI cells, with an average PCE of 0.45% and 0.95%, respectively (see Table S2, Supporting Information, also). Importantly, the PCE of CABI+HI device represents a twofold increase than the pristine CABI cells,[15] highlighting the merits of our HI treatment and resultant microstructural enhancement of the CABI layers. The PCE of 1.30% of the champion device is higher than the recently reported value (1%) for CABI solar cells.[18] The current density (*J*)–voltage (*V*) characteristics (forward bias scans) of the champion cells are presented in Figure 3c. The devices show hysteresis between the reverse and forward voltage scans (see Figure S10a,c, Supporting Information), as reported earlier.[15] A brief discussion on the device hysteresis and the steady-state performance of the devices is presented in Figure S10b,d, Supporting Information. Clearly, upon HI addition into CABI precursor solution, the PCE of these devices is doubled, mostly due to increased J_{SC} and V_{OC} (Figure 3b). The reason for such enhancement (also observed in the indoor light study discussed below) could be partially found in the verified improved morphology as well as surface coverage (Figure 1d) of CABI+HI film, which reduces the incident photon losses.[23,26] Furthermore, it has been shown that the addition of excess iodide ions to precursor solutions can fill the iodide vacancies, in turn mitigating the non-radiative losses of both LHPs and PIMs.[10,27] This suggests that, similarly, the addition of HI can passivate the traps of CABI film, as supported by the increased PL intensity and average lifetime of CABI+HI versus CABI (Figure 2a,c) and a little excess iodine detected at CABI+HI film's bulk and surface (Table 1).

The EQE spectra of the devices (Figure 3d) closely match the absorption spectra of CABI and CABI+HI materials. The EQE values are higher for CABI+HI solar cells (nearly 35% at 370 nm and 25% at the bandgap maximum, that is, 500–550 nm) than for the reference CABI device (14% and 8% at 370 nm and at the bandgap maximum, respectively) for all the wavelengths. By comparing the short-current density (J_{SC}) values from EQE measurements (J_{SC}^{EQE}) and *J*–*V* curves (J_{SC}^{J-V}), surprisingly, we observed that J_{SC}^{EQE} (1.28 and 3.97 mA cm^{-2} for CABI and CABI+HI, respectively) was higher than J_{SC}^{J-V} (1.15 and 3.40 mA cm^{-2} for CABI and CABI+HI, respectively), see Figure 3d. To verify the origin of such a mismatch, we have

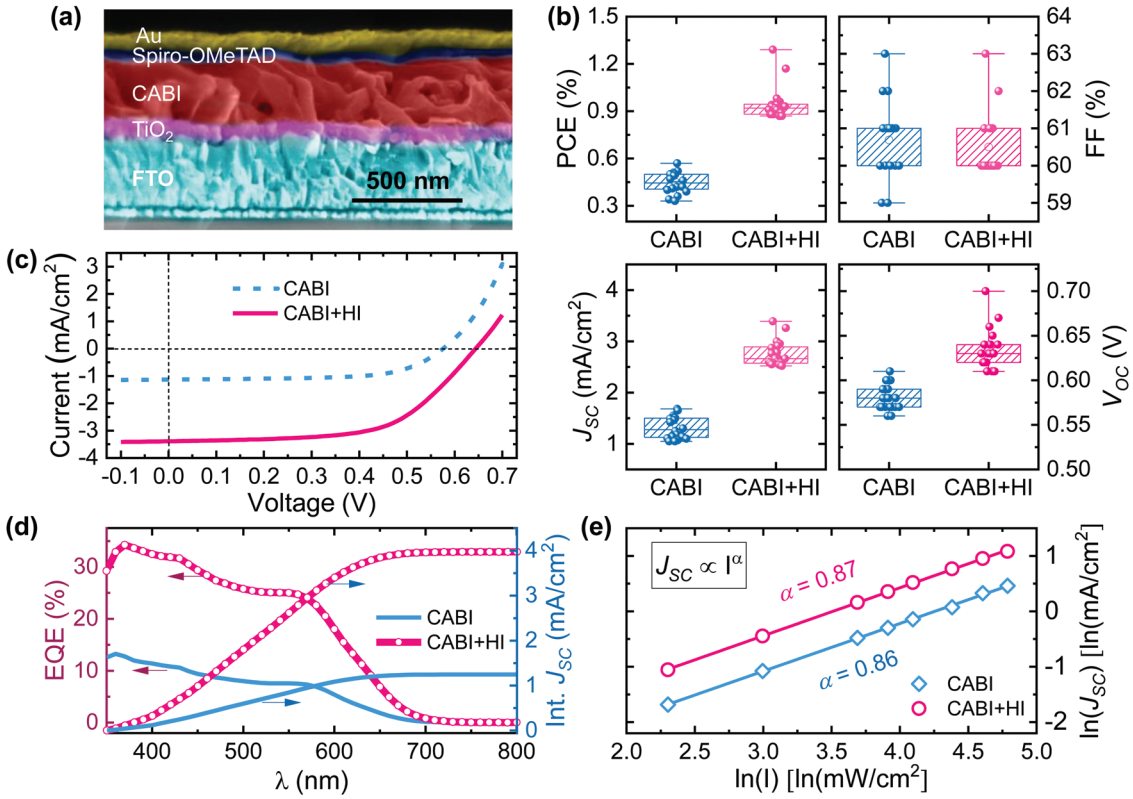

Figure 3. a) Cross-sectional SEM image of a CABI-based solar cell. b) Statistical distribution (over 20 devices) of the photovoltaic parameters of CABI and CABI+HI under 1 sun illumination. c) *J–V* curves (forward bias scans) of CABI and CABI+HI cells. d) EQE spectra of the investigated devices and integrated J_{SC}. e) Log-log plot of J_{SC} versus light intensity for CABI+HI device.

recorded *J–V* scans for CABI and CABI+HI devices with intensity-dependent illumination (10 to 120 mW cm^{-2}).[28] The linear log-log plot of J_{SC} versus light intensity (Figure 3e) reveals the power-law dependence of J_{SC} ($J \propto P^{\alpha}$). The exponent (α) value of $0.87 < 1$ ($\alpha = 0.86$ for pristine CABI device) evidences the sublinear growth of J_{SC} as a function of the optical power. The reduced charge collection efficiency observed at higher light intensities can be attributed to an exponential distribution of defect states within the forbidden gap, according to Rose–Bube's one-center model for $1/2 < \alpha < 1$.[25]

The unencapsulated CABI+HI solar cell retains nearly 85% of its initial PCE after five weeks of storage in air (Figure S11, Supporting Information). Both $V_{OC}$and FF remain nearly constant during this period, after a slight initial increase. The efficiency drop is mainly attributed to a loss in J_{SC}, which might be related to the degradation of CABI at the CABI|Spiro-OMeTAD interface. This stability trend is similar to that of the recently reported CABI solar cells and other lead-free PIMs such as $Cs_3Sb_2I_9$.[11,18] Future studies may focus on: i) improving the stability of CABI devices under different testing conditions; and/or ii) investigating the effect of the impurity phase present in CABI on the device stability. In addition to the shelf-life stability, we monitored the efficiency of the unencapsulated CABI+HI device in air (RH ≈ 50%) at the maximum power point (MPP) under continuous 1 sun illumination. The device retained 97% and 80% of initial efficiency after 60 and 150 min of the maximum power point (MPP) tracking, respectively (Figure S12, Supporting Information). The *J–V* characteristics of CABI and CABI+HI devices were then recorded under WLED (1000 lux) illumination (**Figure 4**a) and the statistical distribution of the photovoltaic parameters illustrated in Figure 4b (see Table S3, Supporting Information, also). While CABI+HI devices showed an iPCE as high as 4.7% (average 3.7%), the highest iPCE of 2.3% was achieved from CABI cells (average 1.3%). The ≈5% PCE value of the champion CABI+HI device is on par with the performance under 1000 lux indoor illumination of state-of-the-art PIM solar cells (Figure S13, Supporting Information).[8,14]

The fourfold PCE increment from 1.3% (1 sun) to 4.7% (WLED) is consistent with the better match between the EQE spectrum of CABI+HI devices and the spectrum of WLED light (Figure 4c) and sublinear power dependence of J_{SC} of the devices, which benefits photovoltaic operation at low light intensities.

2.3. Loss Analysis of CABI+HI IPVs

To understand the limiting factors of device performance, we examined the changes of the photovoltaic parameters, that is, V_{OC}, FF and J_{SC}, under variable indoor light intensities (between 100 and 45 000 lux, i.e., ≈50 µW cm^{-2} and 18 mW cm^{-2}) (Figure 4d,e).

The slope of the V_{OC} variation in Figure 4d corresponds to $n_{ID}k_BT/q$[8,29] and is equal to $1.6k_BT/q$, where n_{ID} is the

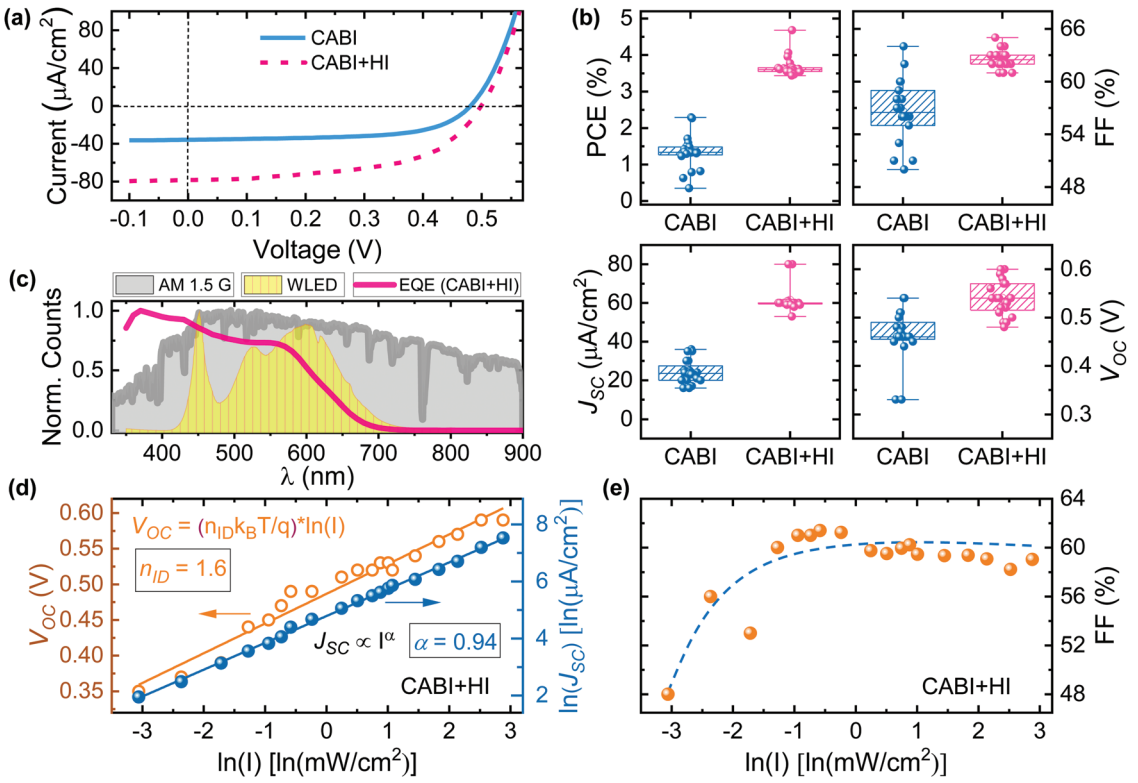

Figure 4. a) *J–V* curves (forward bias scans) of CABI and CABI+HI cells under WLED illumination. b) The statistical distribution (20 devices) of the photovoltaic parameters of CABI and CABI+HI. c) Comparison between the EQE spectrum of CABI+HI cell, AM 1.5G and WLED spectra (right). d) Changes in V_{OC} and J_{SC} versus light intensity for CABI+HI device. e) J_{SC} variation with WLED light intensity for CABI+HI device.

ideality factor, and k_B, T and q are Boltzmann's constant, temperature and elementary charge, respectively. As $n_{ID} > 1$, this suggests the Shockley-Read-Hall-type trap-assisted recombination (mid gap state-involved bimolecular reaction) in the CABI+HI absorber.[8,30] The n_{ID} value of 1.2 obtained under 0.1–1.0 sun conditions for CABI+HI device might suggest that interfacial recombination affects the higher light intensity regime; however, the bulk defects dominate the lower intensity regime.[29] Notably, the highest V_{OC} of 0.6 V extracted from one of CABI+HI cells is higher than the V_{OC} values reported for the best performing rudorffite and $Cs_3Sb_2Cl_xI_{9-x}$ PIM solar cells under indoor illumination (1000 lux).[8,14] The J_{SC} variation with WLED light intensity ($J \propto P^{\alpha}$) in Figure 4d follows the above-discussed AM1.5 light intensity trend with an α value of 0.94. Indeed, the slope of the photocurrent-intensity characteristics on log-log scale is 0.87 in the high-power range (AM1.5 illumination) and 0.94 in the low-power range (WLED illumination). Given that the slope of such characteristics can be traced to the particular recombination mechanism in place,[31] the observed slope difference in different optical power ranges suggests an interplay of two different recombination mechanisms, with their weight changing as the intensity is varied. Given that the slope is reduced at higher power densities and that the behavior at lower power densities is nonetheless sublinear, we trace the observed behavior to the dominance of a recombination mechanism involving a distribution of defects states varying in energy at low light intensities, with bimolecular recombination acquiring greater weight at higher light intensities.[31]

The FF decreases when lowering the WLED intensity (as for V_{OC}) owing to a lower charge carrier formation at a lower light intensity (Figure 4e). Shunt paths across the devices outweigh the FF losses at low light intensities.[29,32] The shunt resistance values (≈2–3 × 10^3 Ω) extracted from dark *J–V* curves (see Table S2, Supporting Information) are low, likely because of the still nonoptimal morphology with pinholes or voids (Figure 1d) in CABI and CABI+HI films, which can enable direct contact between the HTL and ETL in the cell. Hence, while improvements in J_{SC} and V_{OC} are noted when switching from CABI to CABI+HI devices, on average the FF does not significantly change under both 1 sun and WLED illuminations. The increase in V_{OC} values may be attributed to the lower interfacial recombination losses,[33] as supported by the slightly higher hole injection yield for CABI+HI versus CABI thin films (Table S1, Supporting Information). Defect passivation strategies should be considered to further suppress the non-radiative recombination losses, in turn enhancing both FF and V_{OC}.

Furthermore, IPV market is the fastest growing non-traditional PV market and by 2023 it is expected to reach a value of $850 million.[34] The manufacturing costs of perovskite PVs (31.7 $\$m^{-2}$) is already lower than those of c-Si (76 $\$m^{-2}$). However, minimizing the cost further is essential for perovskite IPV-based product viability in market. In the view of

minimizing the fabrication costs, CABI represents an interesting alternative for PV-powered IoT devices.

3. Conclusions

In conclusion, we explored for the first time the use of HI additive to enhance the film morphology and increase the surface coverage of Cu_2AgBiI_6 (CABI) PIM films. This led to improved optical properties and reduced interfacial recombination. When n-i-p photovoltaic cells with CABI+HI absorbers were developed, the champion device reached a PCE of 1.3% under solar illumination, which is the highest efficiency achieved for CABI solar cells so far. Importantly, given the bandgap of CABI that better matches the spectrum of typical indoor lights, we studied, for the first time, the development of CABI-based IPVs. The devices with CABI+HI exhibited an iPCE of up to 4.7% with the highest ever-reported V_{OC} (0.6 V) for a PIM-based IPV cell. Our devices already reached an iPCE within the same range of the commercially dominant a-Si:H IPV. The successful adoption of additive engineering to enhance the microstructure and photovoltaic performance of CABI points to the potential of future efforts in this direction to allow CABI to approach its ultimate efficiency limit of 50–60% and thus enable low-toxicity high-performance IPVs.

Supporting Information

Supporting Information is available from the Wiley Online Library or from the author.

Acknowledgements

This work made use of Tampere Microscopy Center facilities at Tampere University. This work is part of the Academy of Finland Flagship Programme, Photonics Research and Innovation (PREIN), Decision No. 320165. P.V. acknowledges the financial support from the Jane and Aatos Erkko foundation through the SOL-TECH project. M.L. thanks the Finnish Cultural Foundation (No. 00220107) for funding.

Conflict of Interest

The authors declare no conflict of interest.

Data Availability Statement

The data that support the findings of this study are available from the corresponding author upon reasonable request.

Keywords

additive engineering, Cu_2AgBiI_6, film morphology, indoor photovoltaics, perovskite-inspired materials

Received: June 17, 2022
Published online:

[1] I. Mathews, S. N. Kantareddy, T. Buonassisi, I. M. Peters, *Joule* **2019**, *3*, 1415.
[2] M. Freunek, M. Freunek, L. M. Reindl, *IEEE J. Photovoltaics* **2012**, *3*, 59.
[3] M. Freitag, J. Teuscher, Y. Saygili, X. Zhang, F. Giordano, P. Liska, J. Hua, S. M. Zakeeruddin, J.-E. Moser, M. Grätzel, A. Hagfeldt, *Nat. Photonics* **2017**, *11*, 372.
[4] H. K. H. Lee, J. Wu, J. Barbé, S. M. Jain, S. Wood, E. M. Speller, Z. Li, F. A. Castro, J. R. Durrant, W. C. Tsoi, *J. Mater. Chem. A* **2018**, *6*, 5618.
[5] C. Dong, X. Li, C. Ma, W. Yang, J. Cao, F. Igbari, Z. Wang, L. Liao, *Adv. Funct. Mater.* **2021**, *31*, 2011242.
[6] V. Pecunia, L. G. Occhipinti, R. L. Z. Hoye, *Adv. Energy Mater.* **2021**, *11*, 2100698.
[7] Y.-T. Huang, S. R. Kavanagh, D. O. Scanlon, A. Walsh, R. L. Z. Hoye, *Nanotechnology* **2021**, *32*, 132004.
[8] Y. Peng, T. N. Huq, J. Mei, L. Portilla, R. A. Jagt, L. G. Occhipinti, J. L. MacManus-Driscoll, R. L. Z. Hoye, V. Pecunia, *Adv. Energy Mater.* **2021**, *11*, 2002761.
[9] L. C. Lee, T. N. Huq, J. L. MacManus-Driscoll, R. L. Z. Hoye, *APL Mater.* **2018**, *6*, 084502.
[10] K. M. Boopathi, P. Karuppuswamy, A. Singh, C. Hanmandlu, L. Lin, S. A. Abbas, C. C. Chang, P. C. Wang, G. Li, C. W. Chu, *J. Mater. Chem. A* **2017**, *5*, 20843.
[11] A. Hiltunen, N. Lamminen, H. Salonen, M. Liu, P. Vivo, *Sustainable Energy Fuels* **2022**, *6*, 217.
[12] I. Turkevych, S. Kazaoui, E. Ito, T. Urano, K. Yamada, H. Tomiyasu, H. Yamagishi, M. Kondo, S. Aramaki, *ChemSusChem* **2017**, *10*, 3754.
[13] K. Rühle, M. Kasemann, in *2013 IEEE 39th Photovolt. Spec. Conf*, IEEE, Piscataway, NJ **2013**, pp. 2651.
[14] I. Turkevych, S. Kazaoui, N. Shirakawa, N. Fukuda, *Jpn. J. Appl. Phys.* **2021**, *60*, SCCE06.
[15] H. C. Sansom, G. Longo, A. D. Wright, L. R. V. Buizza, S. Mahesh, B. Wenger, M. Zanella, M. Abdi-Jalebi, M. J. Pitcher, M. S. Dyer, T. D. Manning, R. H. Friend, L. M. Herz, H. J. Snaith, J. B. Claridge, M. J. Rosseinsky, *J. Am. Chem. Soc.* **2021**, *143*, 3983.
[16] L. R. V. Buizza, A. D. Wright, G. Longo, H. C. Sansom, C. Q. Xia, M. J. Rosseinsky, M. B. Johnston, H. J. Snaith, L. M. Herz, *ACS Energy Lett.* **2021**, *6*, 1729.
[17] J. Mei, M. Liu, P. Vivo, V. Pecunia, *Adv. Funct. Mater.* **2021**, *31*, 2106295.
[18] F. Zhang, Z. Hu, B. Zhang, Z. Lin, J. Zhang, J. Chang, Y. Hao, *ACS Appl. Mater. Interfaces* **2022**, *14*, 18498.
[19] C. Xiao, Z. Li, H. Guthrey, J. Moseley, Y. Yang, S. Wozny, H. Moutinho, B. To, J. J. Berry, B. Gorman, *J. Phys. Chem. C* **2015**, *119*, 26904.
[20] J. Zhu, L. Zhou, Y. Zhu, J. Huang, L. Hou, J. Shen, S. Dai, C. Li, *Small* **2022**, *18*, 2104399.
[21] L. Vitos, A. V. Ruban, H. L. Skriver, J. Kollár, *Surf. Sci.* **1998**, *411*, 186.
[22] U. H. Hamdeh, R. D. Nelson, B. J. Ryan, U. Bhattacharjee, J. W. Petrich, M. G. Panthani, *Chem. Mater.* **2016**, *28*, 6567.
[23] A. Dualeh, N. Tétreault, T. Moehl, P. Gao, M. K. Nazeeruddin, M. Grätzel, *Adv. Funct. Mater.* **2014**, *24*, 3250.
[24] G. E. Eperon, S. D. Stranks, C. Menelaou, M. B. Johnston, L. M. Herz, H. J. Snaith, *Energy Environ. Sci.* **2014**, *7*, 982.
[25] V. Pecunia, Y. Yuan, J. Zhao, K. Xia, Y. Wang, S. Duhm, L. Portilla, F. Li, *Nano-Micro Lett.* **2020**, *12*, 27.
[26] S. Agarwal, P. R. Nair, *J. Appl. Phys.* **2017**, *122*, 163104.
[27] M. Abdi-Jalebi, Z. Andaji-Garmaroudi, S. Cacovich, C. Stavrakas, B. Philippe, J. M. Richter, M. Alsari, E. P. Booker, E. M. Hutter, A. J. Pearson, S. Lilliu, T. J. Savenije, H. Rensmo, G. Divitini, C. Ducati, R. H. Friend, S. D. Stranks, A. J. Pearson, *Nature* **2018**, *555*, 497.

[28] B. Ghosh, B. Wu, X. Guo, P. C. Harikesh, R. A. John, T. Baikie, A. T. S. Wee, C. Guet, T. C. Sum, S. Mhaisalkar, N. Mathews, *Adv. Energy Mater.* **2018**, *8*, 1802051.
[29] D. Glowienka, Y. Galagan, *Adv. Mater.* **2022**, *34*, 2105920.
[30] W. Tress, M. Yavari, K. Domanski, P. Yadav, B. Niesen, J. P. C. Baena, A. Hagfeldt, M. Graetzel, *Energy Environ. Sci.* **2018**, *11*, 151.
[31] A. Rose, *Concepts in Photoconductivity and Allied Problems*, Interscience Publishers, New York **1963**.
[32] N. Wu, Y. Wu, D. Walter, H. Shen, T. Duong, D. Grant, C. Barugkin, X. Fu, J. Peng, T. White, K. Catchpole, K. Weber, *Energy Technol.* **2017**, *5*, 1827.
[33] L. Canil, J. Salunke, Q. Wang, M. Liu, H. Köbler, M. Flatken, L. Gregori, D. Meggiolaro, D. Ricciarelli, F. De Angelis, M. Stolterfoht, D. Neher, A. Priimagi, P. Vivo, A. Abate, *Adv. Energy Mater.* **2021**, *11*, 2101553.
[34] C. Polyzoidis, K. Rogdakis, E. Kymakis, *Adv. Energy Mater.* **2021**, *11*, 2101854.